Effects of infinite-range interaction on the localization properties of one-dimensional disordered harmonic chains

Wanwan Shi [*]
School of Physics and Technology, Nanjing Normal University, Nanjing 210023, People's Republic of China

Peiqing Tong [†]
School of Physics and Technology, Nanjing Normal University, Nanjing 210023, People's Republic of China; Jiangsu Key Laboratory for Numerical Simulation of Large Scale Complex Systems, Nanjing Normal University, Nanjing 210023, People's Republic of China; and Nanjing Normal University Taizhou College, Taizhou 225300, People's Republic of China

(Received 17 March 2023; revised 29 May 2023; accepted 29 June 2023; published 12 July 2023)

We study the effects of infinite-range (IR) interaction on the localization properties of one-dimensional disordered harmonic chains. Two kinds of disordered models are considered: one is with disordered masses, but constant spring coefficient (mass model), and the other is with disordered spring coefficient, but constant mass (spring model). It is found that the IR interaction induces a gap between the $\omega = 0$ and the excited frequency band for both types of disordered models, and their gaps are both proportional to the IR interaction coefficient γ for larger γ. In addition, the width of the excited frequency band of the mass model is also proportional to γ for larger γ, while that of the spring model is independent of γ. By employing the normalized participation ratio, we find that the low-frequency modes of the mass model except for the lowest frequency change from extended to localized states, while the localized properties of the spring model modes remain unchanged. We also discuss the effects of IR interaction on the dynamic behaviors of the two kinds of disordered models.

DOI: 10.1103/PhysRevB.108.024202

I. INTRODUCTION

Disordered systems and their intrinsic physical laws are important research topics in condensed matter and statistical physics. In 1958, the famous Anderson localization phenomenon was reported in disordered electronic systems [1]. Subsequently, Dean's study of "vibrations of glasslike disordered chains" showed that the lattice modes are localized when disorder exists in a system [2]. However, it is different from the exponential localization of all states of the one-dimensional disordered electronic system [1,3]. For example, there are $\sqrt{N}$ (N is the length of the chain) low-frequency modes that are not localized [4,5]. Recently, there have been a large number of studies on the localization of eigenmodes of various types of inhomogeneous systems. These inhomogeneous systems include quasiperiodic [6–8], random-dimer [9–11], correlated disordered systems [12–16], etc. However, these systems only contain short-range (SR) interaction.

On the other hand, long-range (LR) interaction exists in a large number of systems, for example, two-dimensional hydrodynamics [17,18], charged [19], and dipolar systems [20]. Interestingly, these systems exhibit properties that are different from those of SR systems, such as ensemble inequality [21–23] and the possibility of negative specific heat under the microcanonical ensemble [21]. Due to these particular properties, a great deal of research has been done within LR interaction systems in recent years [24–27], for example, the localization transition of phonon systems with power-law decaying interaction [28], the thermalization of Fermi-Pasta-Ulam-Tsingou models with power-law decaying nonlinear interaction [29] and isolated harmonic networks under conservative noise [30], and the heat conduction of phonon systems with the inverse-square decay and exponential decay [31]. It is commonly believed that the LR interaction can induce the rapid spreading of information [32] and the destruction of localization [33]. However, recently, Celardo *et al.* studied the effect of a special class of LR interaction (infinite-range interaction) on electronic localization states [34,35]. It was found that infinite-range (IR) interaction does not change the properties of the localization of the excited states and they call this phenomenon the cooperative shielding effect. In addition, systems with IR interactions are often employed as theoretical models to study the particular properties of LR systems. Typical examples include the Sherrington-Kirkpatrick model [36], the Lipkin-Meshkov-Glick model [37], and the Hamiltonian mean-field model [24,38]. Moreover, infinite-range interactions can be achieved in ion traps [39–41] and cold atoms coupled to photonic crystals [42] in the laboratory.

Since disorder affects the localization properties of phonon modes differently from that of the electrons, it is an interesting issue to study the effect of IR interaction on the localization properties of disordered phonon modes. In this paper, we focus on how the IR interaction affects the frequency spectrum,

[*]wanwanshi@njnu.edu.cn
[†]Corresponding author: pqtong@njnu.edu.cn

localization of eigenmodes, and dynamic behavior of waves of one-dimensional disordered harmonic chains. Two types of disordered models, i.e., the mass model and the spring model, are considered. Using matrix diagonalization, we obtain the eigenfrequencies and eigenmodes of the systems. To analyze the spatial extension of the eigenmodes, we use the time-independent normalized participation ratio to characterize the localized property of the systems. In dynamics, we study the time evolution of a localized energy pulse and employ the fraction of the total energy and the participation number $\xi(t)$ to evaluate the localized properties of the wave. The paper is organized as follows: in Sec. II, we introduce the Hamiltonian of the system, the eigenequations, and their eigenfrequencies of two kinds of disordered models. In Secs. III and IV, we illustrate the effect of IR interaction on the localization properties of the two kinds of disordered models by the time-independent normalized participation ratio and dynamics of the localized energy pulse, respectively. In Sec. V, a short conclusion is presented.

II. HAMILTONIAN AND EIGENFREQUENCY

Let us consider a general one-dimensional (1D) atomic chain of N atoms with nearest-neighbor interaction and IR interaction. The Hamiltonian is given by

$$H=\sum_{n=1}^{N}\left[\frac{p_n^2}{2m_n}+\frac{1}{2}\beta_n(\mu_n-\mu_{n-1})^2+\frac{\gamma}{2N}\sum_{l=0}^{n-1}(\mu_n-\mu_l)^2\right], \tag{1}$$

where μ_n is the displacement of the nth atom from the equilibrium position. Here, m_n is the mass of the nth atom, β_n is the spring coefficient between the nth to $(n-1)$th atoms, and γ is the IR interaction coefficient.

The equation of motion for the displacements μ_n is

$$\begin{aligned} m_n\ddot{\mu}_n =& -(\beta_n+\beta_{n+1})\mu_n+\beta_n\mu_{n-1}+\beta_{n+1}\mu_{n+1} \\ &-\gamma\mu_n+\frac{\gamma}{N}\sum_{l=1}^{N}\mu_l. \end{aligned} \tag{2}$$

Substituting the formal solution $\mu_n(t)=\mu_n e^{i\omega t}$ into Eq. (2), we obtain the stationary equation of motion,

$$\begin{aligned} \omega^2 m_n\mu_n =& (\beta_n+\beta_{n+1})\mu_n-\beta_n\mu_{n-1}-\beta_{n+1}\mu_{n+1} \\ &+\gamma\mu_n-\frac{\gamma}{N}\sum_{l=1}^{N}\mu_l. \end{aligned} \tag{3}$$

The matrix form can be expressed as

$$\omega^2 M\mu=H\mu, \tag{4}$$

where ω and $\mu=(\mu_1,\ldots,\mu_N)^T$ are the eigenfrequencies and the corresponding eigenmodes, respectively. $M=\mathrm{diag}(m_1,\ldots,m_N)$ is a diagonal matrix, and H is a $N\times N$ secular matrix defined as $H_{n,n}=\beta_n+\beta_{n+1}+\gamma-\gamma/N$, $H_{n,n+1}=H_{n+1,n}=H_{1,N}=H_{N,1}=-\beta_{n+1}-\gamma/N$, and all other $H_{n,m}=-\gamma/N$. The periodic boundary conditions are employed.

For simplicity, we choose two types of widely studied and inequivalent disordered models. One is with disordered masses but constant spring coefficient $\beta_n=\beta=1$ (mass model) [7,8], and the other is with disordered spring coefficient but constant mass $m_n=m=1$ (spring model) [11,12].

For the mass model, m_n is the random number uniformly distributed in $[m_1,m_2]$, where $m_2>m_1>0$. Without loss of generality, we take the average value of the m_n as 1. The disorder strength $\delta m=m_2-m_1$. The matrix M can be written as two matrices $M=LL^T$ by Cholesky decomposition [43]. Therefore, Eq. (4) can be rewritten as

$$\omega^2\widetilde{\mu}=\widetilde{H}\widetilde{\mu}, \tag{5}$$

where $\widetilde{\mu}=L^T\mu$, $\widetilde{H}=L^{-1}H(L^T)^{-1}$.

For the spring model, β_n is the random number uniformly distributed in $[\beta_1,\beta_2]$, where $\beta_2>\beta_1>0$. Likewise, we take the average value of the spring coefficient β_n as 1, and the disorder strength $\delta\beta=\beta_2-\beta_1$. Equation (4) can be rewritten as

$$\omega^2\mu=\frac{H}{m}\mu. \tag{6}$$

Let us first consider the case of a homogenous system ($\beta_n=\beta$ and $m_n=m$). Due to the existence of translational invariance of the homogeneous system, the μ_n has the form Ae^{-iqn}. Here, for finite N, $q=2\pi\frac{h}{N}$ and $-[\frac{N}{2}]\leqslant h<[\frac{N}{2}]$. Substituting the form solution of $\mu_n(t)$ into Eq. (3), we can get the frequency of the homogeneous harmonic chain with IR interaction

$$\omega^2=\frac{4\beta}{m}\sin^2\left(\frac{q}{2}\right)+\frac{\gamma}{m}(1-\delta_{q0}), \tag{7}$$

where the $\delta_{q0}=1$ for $q=0$, else $\delta_{q0}=0$.

It follows that there is a gap $\sqrt{\gamma/m}$ between the lowest-frequency $\omega_0=0$ and the excited frequency band in the limit of N tending to infinity. And the width of the excited frequency band is $\sqrt{4\beta/m}$. For convenience, we use $\Delta G(\omega^2)=\omega_1^2-\omega_0^2$ (ω_1 corresponding to the first excited frequency) and $\Delta\Omega(\omega^2)=\omega_{N-1}^2-\omega_1^2$ to describe the gap and the width of the excited frequency band in the following. Therefore, for the homogenous system, $\Delta G(\omega^2)=\gamma/m$ and $\Delta\Omega(\omega^2)=4\beta/m$ in the limit of N tending to infinity.

Now let us analyze the results of the disordered systems. In the following, we will discuss the effect of IR interaction on the gap $\Delta G(\omega^2)$ and the width $\Delta\Omega(\omega^2)$ of the excited frequency band for the two kinds of disordered models. First, we discuss the results of the mass model. In Figs. 1(a) and 1(c), the $\Delta G(\omega^2)$ and $\Delta\Omega(\omega^2)$ as functions of γ for different N are given, respectively. From Fig. 1(a), it can be seen that $\Delta G(\omega^2)$ of the mass model is constant with γ when γ is small and increases linearly after going through the crossover region. For larger γ, the curves of different N overlap as one, and $\Delta G(\omega^2)\simeq k_1\gamma$. This is similar to that of the homogeneous system, where $\Delta G(\omega^2)=\gamma/m$ [44]. In the inset of Fig. 1(a), we plot $\Delta G(\omega^2)$ of the homogeneous system and the mass model as functions of γ and find that the coefficient $k_1<1/\overline{m}$, where $\overline{m}$ is the averaged mass of the mass model. This means the $\Delta G(\omega^2)$ of the mass model is smaller than that of the homogeneous model for larger γ. From Fig. 1(c), the $\Delta\Omega(\omega^2)$ is constant when γ is small and increases linearly after the crossover region. And, for any γ, the $\Delta\Omega(\omega^2)$ curves for different N overlap into one. In addition, at large γ, the

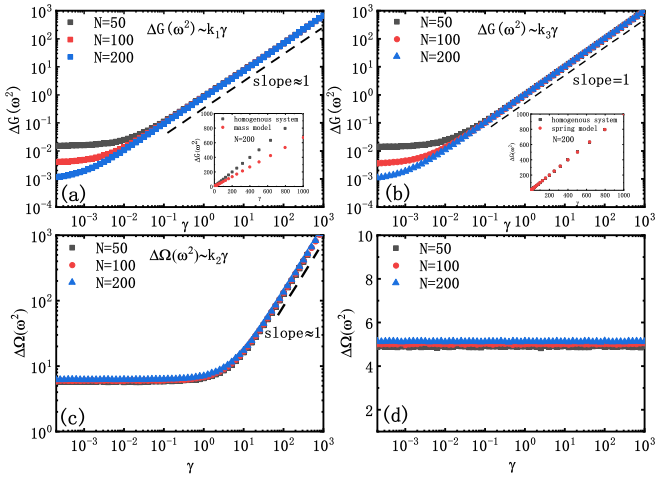

FIG. 1. (a),(b) The gap $\Delta G(\omega^2)$ as functions of γ for mass and spring models, respectively. For comparison, the $\Delta G(\omega^2)$ for the mass model and the spring model with the homogeneous system are given in the insets of (a) and (b), respectively. (c),(d) The width of the excited frequency band $\Delta\Omega(\omega^2)$ as functions of γ for mass and spring models, respectively. Here, $\delta m = 1$ and $\delta\beta = 1$.

$\Delta\Omega(\omega^2)$ approximates as $k_2\gamma$. This is quite different from the results of the homogeneous system in which $\Delta\Omega(\omega^2)$ is a constant. These results can be understood by considering a simplest inhomogeneous model, i.e., period-two mass model. In that model, m_n takes m_1 and m_2 periodically, i.e., $m_{2n} = m_2$, $m_{2n+1} = m_1$. In Appendix A 1, we analyze the frequency of the period-two mass model and obtain that its $\Delta G(\omega^2)$ approximate as γ/m_2 for large γ, where $m_2 > \overline{m}$ [$\overline{m} = \frac{1}{2}(m_1 + m_2)$]. And the $\Delta\Omega(\omega^2)$ approximates as $2\beta(m_2 + m_1)/m_1m_2$ for $\gamma \ll 2\beta$, which is independent of γ, while for $\gamma \gg 2\beta$, the $\Delta\Omega(\omega^2)$ approximate as $\gamma(m_2 - m_1)/m_1m_2$. This means that the difference between homogeneous and disordered systems comes from the inhomogeneity of the mass.

Then, we discuss the results of the spring model. Figures 1(b) and 1(d) show the $\Delta G(\omega^2)$ and $\Delta\Omega(\omega^2)$ as functions of γ for different N, respectively. From Fig. 1(b), the trend of the curve for the spring model is similar to that of the mass model. The difference is that for larger γ, the $\Delta G(\omega^2)$ for the spring model is approximately equal to that of the homogeneous model [see the inset of Fig. 1(b)], i.e., $\Delta G(\omega^2) \simeq \gamma/m$. In Fig. 1(d), we find that the $\Delta\Omega(\omega^2)$ is independent of γ, which is similar to that of the homogenous system. The results are different from the results of the mass model at larger γ. Similarly, we can understand this result by considering a period-two spring model (i.e., β_n takes two values β_1, β_2 periodically). In Appendix A 2, we get the $\Delta G(\omega^2) = \gamma/m$ and the $\Delta\Omega(\omega^2) = 2(\beta_1 + \beta_2)/m$. This is consistent with the qualitative results of the spring model, indicating that inhomogeneous spring coefficients do not influence the $\Delta G(\omega^2)$. And the $\Delta\Omega(\omega^2)$ is independent of γ.

III. LOCALIZATION OF EIGENMODES

To analyze the spatial extension of the eigenmodes, we employ the normalized participation ratio $P(\omega^2)$, which is defined as

$$P(\omega^2) = \frac{\left(\sum_{n=1}^{N} |\mu_n|^2\right)^2}{N\sum_{n=1}^{N} |\mu_n|^4}. \tag{8}$$

It is clear from this definition that $P(\omega^2)$ will be of the order of 1 for the extended mode and $1/N$ for the localized mode. For the disordered system, we need to average the results of the samples since each sample has different eigenfrequencies. In our calculations, the averaging process is similar to the literature [8], i.e., averaging over a small window $\Delta\omega^2$ on $P(\omega^2)$,

$$\langle P(\omega^2)\rangle = \left[\sum_{y=\omega^2-\Delta\omega^2/2}^{y=\omega^2+\Delta\omega^2/2} P(y)\right]/N_{\omega^2}, \tag{9}$$

where N_{ω^2} is the number of eigenmodes at each window. In the following results, we average over 200 disordered configurations and get similar results for more disordered configurations.

In addition, to study the localized property of excited frequency modes as a function of γ, we calculate the average participation ratio over all excited frequencies, which can be expressed as

$$\overline{P}_{ex} = \frac{1}{M}\sum_{\alpha=1}^{M}\frac{1}{N-1}\sum_{k\geqslant 1} NP_\alpha(\omega_k^2), \tag{10}$$

where M is the number of disordered samples and ω_k is the kth eigenfrequency. To compare the results of the averaged participation ratio over all excited modes with γ for different N, we scale the $\overline{P}_{ex}$ of the localized mode as 1 (independent of N) by averaging $NP(\omega^2)$ in Eq. (10).

A. Mass model

First, we calculate the average normalized participation ratio $\langle P(\omega^2)\rangle$. Figures 2(a) and 2(b) depict the $\langle P(\omega^2)\rangle$ for different N ($\gamma = 100$) and for different γ ($N = 1000$), respectively. It can be seen that for larger γ, despite the different parameters, the systems have $\langle P(\omega^2)\rangle \approx 0$ for the excited frequencies. This means that for larger γ, the modes of the excited frequencies are localized. This is different from that of the SR ($\gamma = 0$) mass model, where $\sqrt{N}$ low-frequency modes are extended and the high-frequency modes are localized [see the inset of Fig. 2(a)]. Further, to illustrate the numerical results, we give, in Figs. 3(a) and 3(b), the eigenmodes of excited frequencies for the IR ($\gamma = 100$) and SR mass models for a typical disorder configuration, respectively. The results are obtained by $N = 100$ and $\delta m = 1$. To visualize the localization of the eigenmodes, we shift the maximum mode for each eigenfrequency to the middle site. From Fig. 3(a), it can be seen that all eigenmodes of the excited frequencies are localized at several different positions for the IR mass model. This is different from the result of the SR mass model [see Fig. 3(b)]. It can be seen that for larger γ, instead of destroying the localization of the mode, the IR interaction makes the mode more localized, which is counterintuitive.

For smaller γ, we show the $\langle P(\omega^2)\rangle$ for different N in Fig. 2(c). It can be seen that when γ is small, the localization property of the modes is similar to that of the SR mass model.

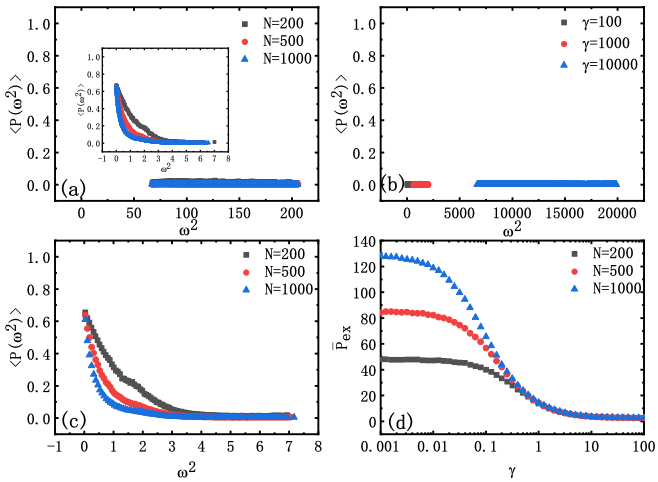

FIG. 2. Mass model: (a),(c) The $\langle P(\omega^2)\rangle$ for different N at $\gamma = 100$ and $\gamma = 0.001$, respectively. The inset of (a) is the $\langle P(\omega^2)\rangle$ of the SR system at different N. (b) The $\langle P(\omega^2)\rangle$ for different γ at $N = 1000$. (d) The average participation ratio $\overline{P}_{ex}$ over the excited frequencies vs γ at different N. The above results are obtained by $\delta m = 1$.

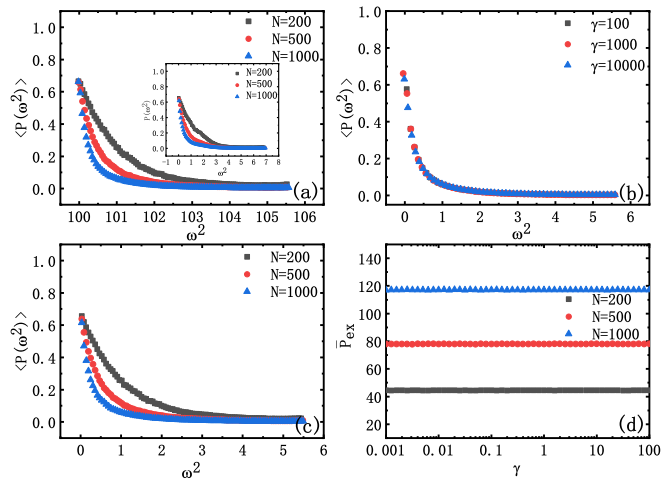

FIG. 4. Spring model: (a)(c) The $\langle P(\omega^2)\rangle$ for different N at $\gamma = 100$ and $\gamma = 0.001$, respectively. The inset of (a) is the $\langle P(\omega^2)\rangle$ of the SR system for different N. (b) The $\langle P(\omega^2)\rangle$ for different γ at $N = 1000$. In (b), we have subtracted γ from the horizontal coordinate of each curve for reasons stated in the main body. (d) The average participation ratio $\overline{P}_{ex}$ over the excited frequencies vs γ for different N. The above results are obtained by $\delta\beta = 1$.

To see the localized properties of the excited frequency modes as a function of γ, we show in Fig. 2(d) the average participation ratio $\overline{P}_{ex}$ over the excited frequencies as a function of γ for different N. It can be seen that for larger γ, all the points collapse almost to a single line, and $\overline{P}_{ex}$ is the order of magnitude of 1. This means that the excited modes are localized, whereas, for smaller γ, $\overline{P}_{ex}$ is proportional to N. This means that the excited modes are delocalized, similar to the results of the SR system.

In general, IR interaction results in low-frequency modes, except for the lowest frequency from extended to localized.

B. Spring model

Likewise, we first present the results of $\langle P(\omega^2)\rangle$ for spring models. Figures 4(a) and 4(b) depict the $\langle P(\omega^2)\rangle$ for different N ($\gamma = 100$) and for different γ ($N = 1000$), respectively. In Fig. 4(b), we subtract γ from the horizontal coordinate of each curve. Because there is a large gap between the lowest-frequency and the excited frequency band, and the relatively small $\Delta\Omega(\omega^2)$ (similar to that in the SR system), the $\langle P(\omega^2)\rangle$ for the excited frequency modes are difficult to observe. From Figs. 4(a) and 4(b), it can be seen that for larger γ, the low-frequency modes are extended, while the high-frequency modes are localized. This is the same as the localized property of the SR ($\gamma = 0$) spring model modes [see the inset of Fig. 4(a)]. Similarly, we show the eigenmodes of excited frequencies for the IR ($\gamma = 100$) and SR spring models under a typical disorder configuration in Fig. 5. It can be seen that the localization properties of the eigenmodes of the IR and SR spring models are similar, in that both are extended for the low-frequency modes and localized for the high-frequency modes. This is analogous to the cooperative shield effect in electronic systems, where the IR term seems to be absent [35]. Moreover, it can be seen from Fig. 4(b) that γ does not affect the number of extended modes.

To understand the effect of γ on the localization properties of the system, we give, in Fig. 4(c), the $\langle P(\omega^2)\rangle$ for different N when γ is small. It is observed that the localized nature of

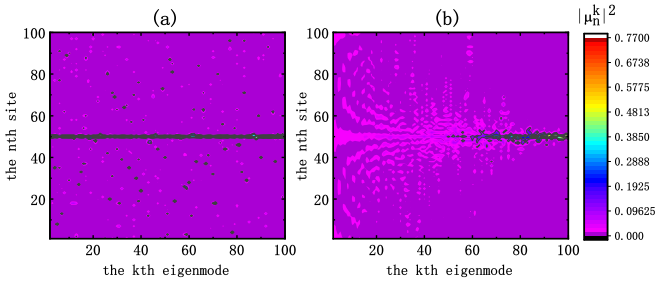

FIG. 3. (a),(b) The eigenmodes $|\mu_n^k|^2$ of excited frequency for the IR ($\gamma = 100$) and SR mass models under a typical disordered configuration, respectively. The common parameters for all panels are $N = 100$ and $\delta m = 1$. The maximum $|\mu_n^k|^2$ corresponding to each frequency is shifted to the middle position.

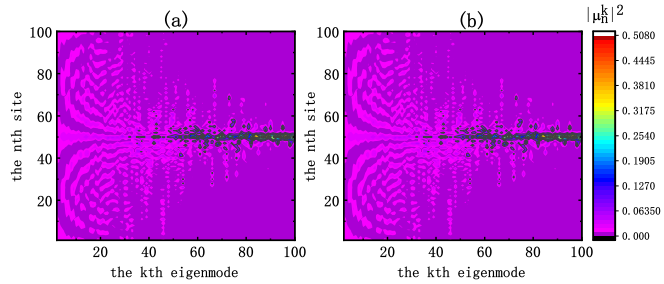

FIG. 5. (a),(b) The eigenmodes $|\mu_n^k|^2$ of the excited frequency for the IR ($\gamma = 100$) and SR spring models under a typical disordered configuration, respectively. The parameters and data processing are the same as the mass model.

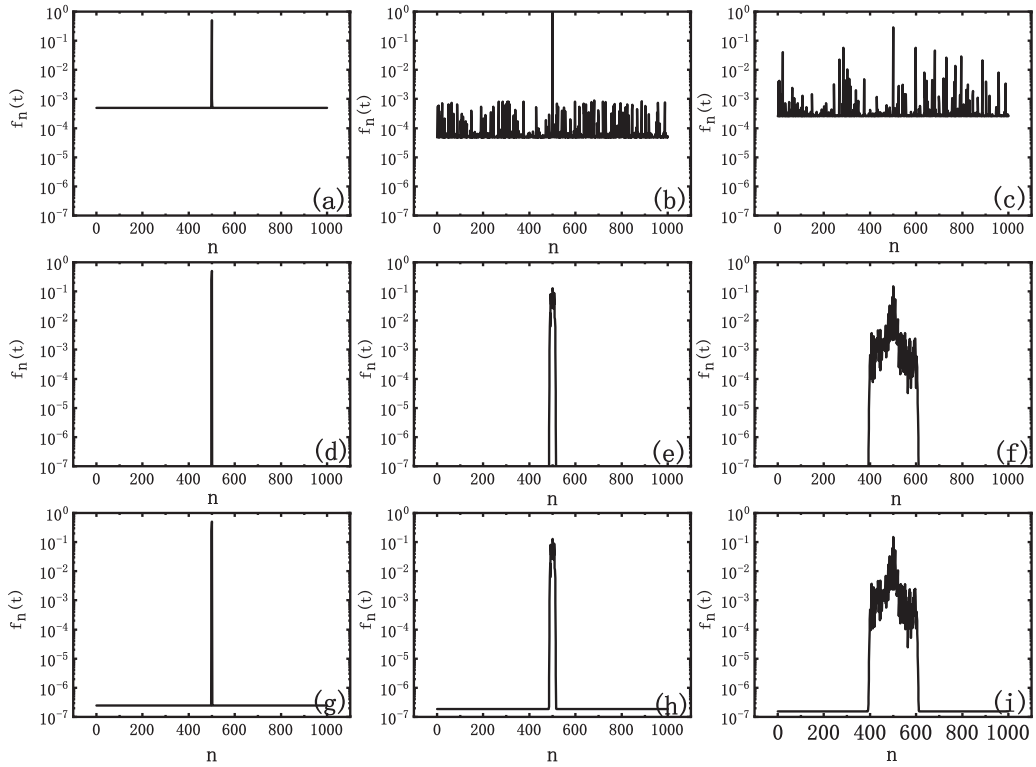

FIG. 6. The f_n as a function of n for the IR mass model with $\gamma = 1000$ at (a) $t = 0.001$, (b) $t = 10$, and (c) $t = 100$, respectively. The results of the SR mass model for corresponding times are shown in (d)–(f), respectively. (g)–(i) The results of the IR mass model with $\gamma = 0.001$ for the corresponding times. The above three systems have the same disordered samples. The results are obtained at $N = 1000$, $\delta m = 1$.

the modes remains the same as that of the SR system. Furthermore, we show, in Fig. 4(d), the average participation ratio $\overline{P}_{ex}$ over the excited frequencies as a function of γ. We can see that $\overline{P}_{ex}$ is always constant for a particular N, indicating that the IR interaction does not modify the localized property of the spring model. In addition, the $\overline{P}_{ex} \propto N$, indicating that the eigenmodes are delocalized modes.

In general, the IR interaction does not change the localized property of the spring model modes, which is quite different from the results of the mass model.

IV. DYNAMICS OF THE LOCALIZED ENERGY PULSE

In this section, we discuss the effects of IR interaction on the property of localization by considering the time evolution of the localized energy pulse [8,10,13,45]. We consider the fraction of the total energy H at site n to be given by $f_n(t) = h_n(t)/H$. The $h_n(t)$ is the "local" energy of the nth atom, which is generally defined as

$$h_n(t) = \frac{p_n^2}{2m_n} + \frac{1}{4}[\beta_{n+1}(\mu_{n+1} - \mu_n)^2 + \beta_n(\mu_n - \mu_{n-1})^2] + \frac{\gamma}{4N}\sum_l (\mu_n - \mu_l)^2. \tag{11}$$

Here, $p_n = m_n\dot{\mu}_n$ and μ_n are the momentum and displacement of the nth atom, respectively. In the following, we employ the generalized time-dependent participation number [45] to describe the localized property of waves, which can be defined as

$$\xi(t) = \frac{1}{\sum_{n=1}^{N} f_n^2(t)}. \tag{12}$$

For the extended energy packet $f_n(t) = 1/N$, it follows that $\xi(t) = N$, while for a localized wave, $\xi(t) = 1$.

We employ the fourth-order Runge-Kutta method to solve Eq. (2). In general, energy transport under initial displacement excitation and initial momentum excitation are considered. Since the results of the two different initial excitations are similar, we only consider the case of the initial displacement excitation $\mu_{N/2}(0) = 1$, $\dot{\mu}_{N/2}(0) = 0$.

A. Mass model

To see the dynamic evolution of the local energy for the IR mass model, we first show, in Figs. 6(a)–6(c), the $f_n(t)$ of the IR mass model with $\gamma = 1000$ for a typical disordered sample at $t = 0.001$, $t = 10$, and $t = 100$, respectively. For comparison, we give, in Figs. 6(d)–6(f), the f_n of the corresponding time for the SR mass model for the same disordered sample. The results of the mass model are obtained by $N = 1000$ and $\delta m = 1$. We can see that the local energy of the IR system ($\gamma = 1000$) is instantaneously transported to other sites and reaches about 10^{-4} at all sites except the initial one. This is a typical feature of the dynamics of the LR interaction system [24]. As time evolves, the energy is gradually localized at several sites. And the sites of localization and the magnitude of localized energy change with time. This is different from the result of the SR system, which is a gradual outward

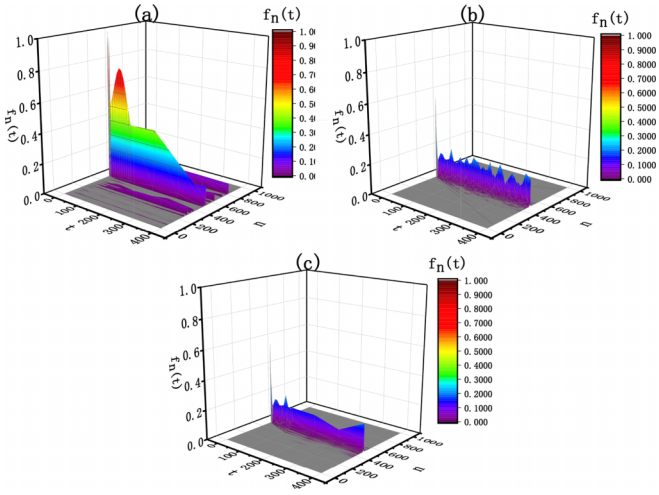

FIG. 7. (a),(c) The three-dimensional diagrams of f_n for the IR mass model with $\gamma = 1000$ and $\gamma = 0.001$ under the same disorder sample at time t in the site n, respectively. (b) For comparison, the results of the SR mass model are given.

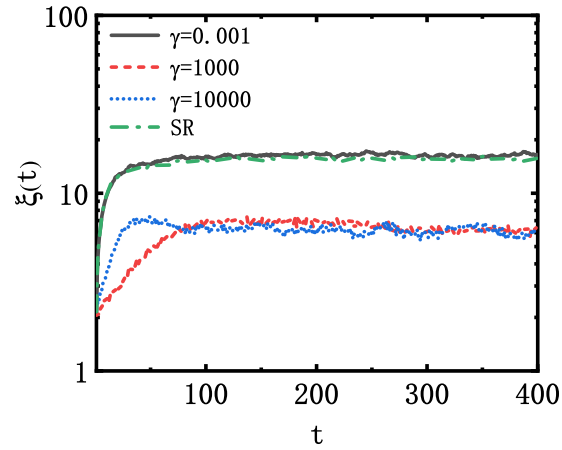

FIG. 8. The average participation number $\xi(t)$ as a function of t at initial displacement excitation. Here the results for different IR interaction coefficients γ are considered, as well as the results for the SR mass model given as a comparison. The results are obtained at $N = 1000$, $\delta m = 1$.

transport of energy. However, most of the energy of the SR mass model is still trapped in the initial site. Moreover, we consider the results of the IR mass model with smaller $\gamma = 0.001$ in Figs. 6(g)–6(i). It can be seen that the local energy of the IR system with smaller $\gamma = 0.001$ is also instantaneously transported to other sites and reaches about 10^{-7} at all sites except the initial one. However, the dynamical behavior of the local energy is similar to that of the SR mass model. To see the process of energy transport globally, we give three-dimensional images of the $f_n(t)$ for the IR ($\gamma = 1000$) and SR mass models in Figs. 7(a) and 7(b), respectively. It can be seen that the energy of the IR system ($\gamma = 1000$) is localized at several different sites, while the SR system gradually transports energy outward except for the energy trapped at the initial site. Figure 7(c) is the three-dimensional image of the IR mass model with smaller $\gamma = 0.001$. It can also be seen that the dynamics of the local energy of the IR mass model with smaller $\gamma = 0.001$ behaves similarly to that of the SR system.

To further understand the localized properties of waves for the IR system, we present the average participation numbers $\xi(t)$ as a function of t for the IR system with different γ, as well as the results for the SR system in Fig. 8. To suppress fluctuations, we employ the results averaged over 200 different disordered configurations. And the averaging of more samples gives similar results. It is observed that both the IR and SR systems saturate at a finite value of $\xi(t)$ due to being dominated by the localized eigenmodes [45]. For the larger γ, it can be seen that $\xi(t)$ of the IR system is smaller than that of the SR system, and the $\xi(t)$ of systems with different γ saturate around the same value. That is, it has more localized waves than that of the SR system (as shown in Figs. 6 and 7). And for the smaller γ, the $\xi(t)$ of its system is similar to that of the SR system. This indicates that smaller γ has no effect on the energy wave transport, in agreement with the static results.

B. Spring model

Likewise, we give the f_n as a function of n for the IR ($\gamma = 1000$) and SR spring model at three different times for a typical disordered sample in Fig. 9. Figures 9(g)–9(i) show the results for the IR spring model with smaller $\gamma = 0.001$ corresponding to times. The results of the spring model are obtained by $N = 1000$ and $\delta\beta = 1$. Similar to the IR mass model, the local energy of the IR spring model ($\gamma = 1000$) is also instantaneously transported to all sites and reaches about 10^{-4} at all sites except the initial site. And for the IR spring model with smaller $\gamma = 0.001$, the local energy is also instantaneously transported to all sites, but the local energy reaches about 10^{-7}. With time evolution, both IR and SR spring models transport energy outward. However, due to the presence of the quasisteady state of the IR system with larger $\gamma = 1000$ [24], the transport process is slow. And the dynamical behavior of the local energy of the spring model with smaller $\gamma = 0.001$ is similar to that of the SR system. Those results can also be obtained from the 3D images of the f_n for the IR and SR spring model (see Fig. 10). In addition, most of the energy of both IR and SR systems is trapped in the initial site, but less energy is trapped in the initial site for the IR system ($\gamma = 1000$) than that of the SR system.

Finally, we show the $\xi(t)$ as a function of t for the spring model with different γ in Fig. 11. As a comparison, we present in the inset the $\xi(t)$ for the SR spring model. It can be seen that similar to the mass model, all systems saturate with $\xi(t)$ at a finite value. The saturation value of the IR system is larger than that of the SR system. This is because, for larger γ, the dynamics behavior of the local energy of the IR and SR systems is more similar, but the IR system has less energy trapped in the initial position (as depicted in Fig. 10). And the value of $\xi(t)$ saturation for the IR system with smaller γ is close to that of the SR system. This is similar to the results of the mass model, where smaller γ has no effect on the transport of energy waves.

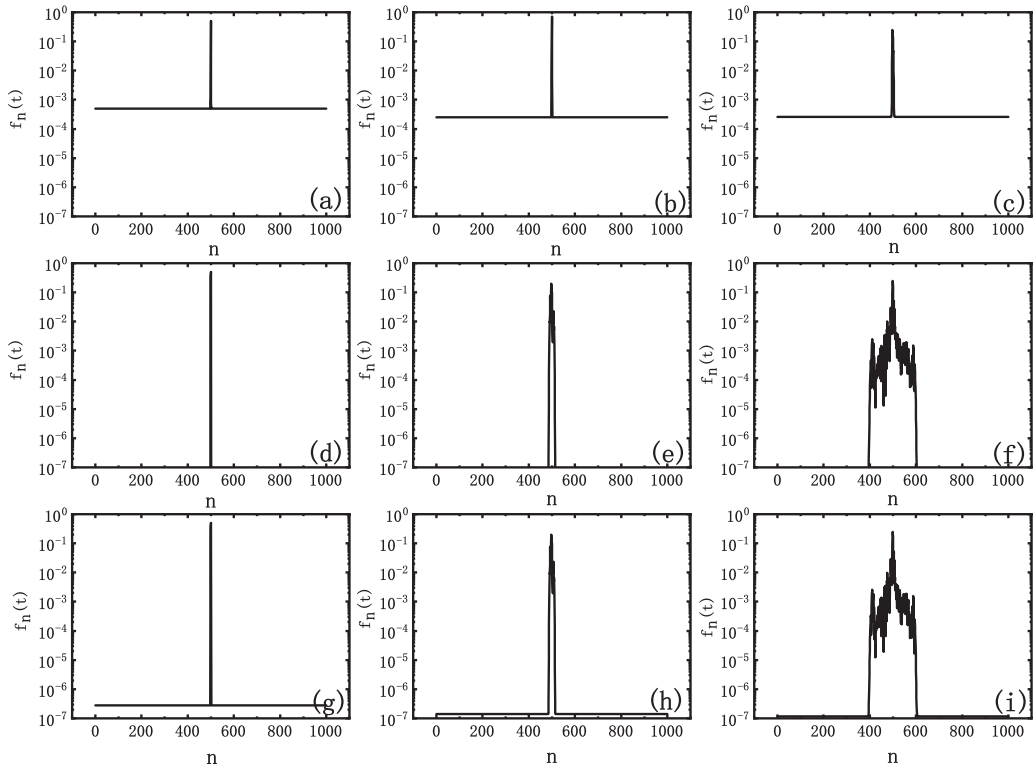

FIG. 9. The f_n as a function of n for the IR spring model with $\gamma = 1000$ at (a) $t = 0.001$, (b) $t = 10$, and (c) $t = 100$, respectively. The results of the SR spring model for corresponding times are shown in (d)–(f), respectively. (g)–(i) The results of the IR spring model with $\gamma = 0.001$ for the corresponding times. The above three systems have the same disordered samples. The results are obtained at $N = 1000$, $\delta\beta = 1$.

V. CONCLUSION

We study the effects of IR interaction on the static and dynamic of one-dimensional disordered harmonic chains. Two kinds of disordered models are considered: the mass model and the spring model. In terms of the frequency spectrum, there is a gap between the lowest-frequency ($\omega_0 = 0$) and the excited frequency band due to IR interaction. For two kinds of disorder models, the gap $\Delta G(\omega^2)$ is proportional to γ for larger γ. Moreover, the width of the excited frequency band $\Delta\Omega(\omega^2)$ of the mass model is also proportional to γ for larger γ. However, $\Delta\Omega(\omega^2)$ of the spring model is independent of γ, which is similar to the case of the homogeneous system.

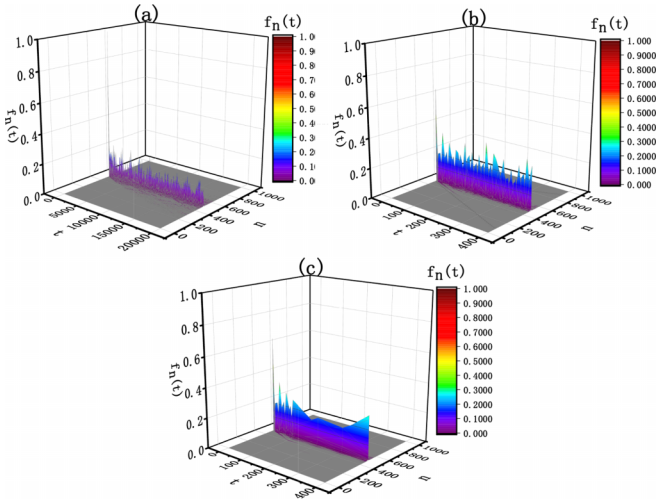

FIG. 10. (a),(c) The three-dimensional diagrams of $f_n(t)$ for the IR spring model with $\gamma = 1000$ and $\gamma = 0.001$ at time t in the site n, respectively. (b) For comparison, the results of the SR spring model are given.

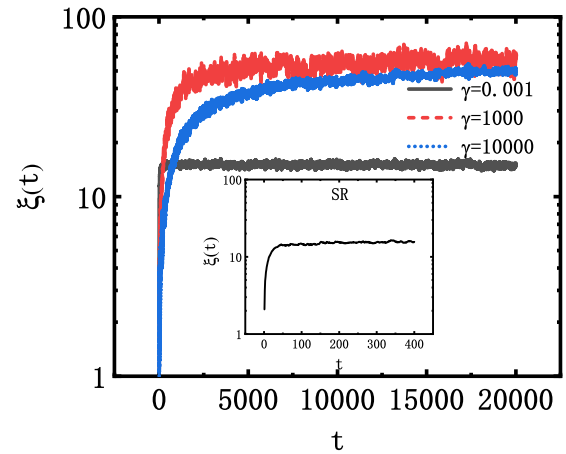

FIG. 11. The average participation number $\xi(t)$ as a function of t at initial displacement excitation. Here the results for different IR interaction coefficients γ are considered. The result of the corresponding SR system is given in the inset as a comparison. The results are obtained at $N = 1000$, $\delta\beta = 1$.

Those results can be understood by analyzing the two kinds of period-two models. For the localized properties of the eigenmodes, the results show that the low-frequency modes of the mass model become localized states for larger γ, except for the lowest frequency, while the localized properties of the eigenmodes of the spring model are not changed. In dynamics, we consider the time evolution of the localized energy pulse. Due to IR interaction, about 10% of the energy is quickly and uniformly distributed over each lattice site, except for the initial site. For the mass model, most of the energy is localized to a number of lattice sites, and the lattice sites vary with time, while for the spring model, most of the energy very slowly spreads from the initial lattice sites to other lattice sites. In short, IR interaction has different effects on the two kinds of disordered models in terms of the frequency spectrum, localization of phonon modes, and wave packet evolution.

ACKNOWLEDGMENTS

The work is supported by the National Natural Science Foundation of China (Grants No. 11975126 and No. 12247106).

APPENDIX: FREQUENCY OF TWO TYPES OF PERIOD-TWO SYSTEMS

Here we analytically obtain the eigenfrequency for the period-two mass and spring models.

1. Period-two mass model

For the period-two mass model, m_n takes two masses periodically, i.e., $m_{2n} = m_2$, $m_{2n+1} = m_1$, where $m_2 > m_1 > 0$. By analogy with Eq. (2), we can obtain the equation of motion for the system with N primitive cells,

$$\begin{aligned} m_2\ddot{\mu}_{2n} &= -\beta(2\mu_{2n} - \mu_{2n+1} - \mu_{2n-1}) - \frac{\gamma}{N}\sum_{l=0}^{2N-1}(\mu_{2n} - \mu_l), \\ m_1\ddot{\mu}_{2n+1} &= -\beta(2\mu_{2n+1} - \mu_{2n+2} - \mu_{2n}) - \frac{\gamma}{N}\sum_{l=0}^{2N-1}(\mu_{2n+1} - \mu_l). \end{aligned} \tag{A1}$$

The equations have lattice wave solution of the following form:

$$\mu_{2n} = Ae^{i[\omega t-(2n)q]}, \quad \mu_{2n+1} = Be^{i[\omega t-(2n+1)q]}. \tag{A2}$$

Substituting the formal solution of Eq. (A2) into Eq. (A1), we can get

$$\begin{aligned} \omega^2 m_2 A &= \beta(2A - 2B\cos q) + \gamma A - \frac{\gamma}{2N}\sum_{n=0}^{N-1}[Ae^{iq(2n)} + Be^{iq(2n+1)}], \\ \omega^2 m_1 B &= \beta(2B - 2A\cos q) + \gamma B - \frac{\gamma}{2N}\sum_{n=0}^{N-1}[Ae^{iq(2n)} + Be^{iq(2n+1)}]. \end{aligned} \tag{A3}$$

Using $\frac{1}{N}\sum_{n=0}^{N-1} e^{i2nq} = \delta_{q0}$, the equation can be expressed as

$$(\omega^2 m_2 - D_1)A + D_2 B = 0, \quad D_2 A + (\omega^2 m_1 - D_1)B = 0, \tag{A4}$$

where $D_1 = D_2 = 2\beta + \frac{\gamma}{2}$ for $q = 0$, and $D_1 = 2\beta + \gamma$ and $D_2 = 2\beta\cos q$ for $q \neq 0$.

So the frequency can be obtained,

$$\omega_{\pm}^2(q) = \frac{(m_1 + m_2)D_1 \pm \sqrt{(m_1 + m_2)^2 D_1^2 - 4m_1 m_2\left(D_1^2 - D_2^2\right)}}{2m_1 m_2}. \tag{A5}$$

For $q = 0$, the frequency is

$$\omega_{\pm}^2(q) = \begin{cases} \dfrac{(m_1 + m_2)\left(2\beta + \frac{\gamma}{2}\right)}{m_1 m_2}, \\ 0. \end{cases} \tag{A6}$$

For $q \neq 0$, the frequency is

$$\omega_{\pm}^2(q) = \frac{D_1(m_1 + m_2) \pm \sqrt{D_1^2(m_1 - m_2)^2 + 4m_1 m_2(2\beta\cos q)^2}}{2m_1 m_2}. \tag{A7}$$

The $\Delta G(\omega^2) = \omega_-^2(q \to 0) - \omega_-^2(q = 0)$ can be written as

$$\Delta G(\omega^2) = \frac{D_1(m_1 + m_2) - \sqrt{D_1^2(m_1 - m_2)^2 + 4m_1m_2(2\beta)^2}}{2m_1m_2}, \tag{A8}$$

where $D_1 = 2\beta + \gamma$. For the large γ, the $\Delta G(\omega^2)$ is

$$\Delta G(\omega^2) \approx \frac{\gamma}{m_2}. \tag{A9}$$

The $\Delta\Omega(\omega^2)$ can be expressed as

$$\Delta\Omega(\omega^2) = \omega_+^2(q \to 0) - \omega_-^2(q \to 0) = \frac{\sqrt{(2\beta + \gamma)^2(m_1 - m_2)^2 + 4m_1m_2(2\beta)^2}}{m_1m_2}. \tag{A10}$$

So, the $\Delta\Omega(\omega^2) \approx \frac{2\beta(m_2+m_1)}{m_1m_2}$ when $\gamma \ll 2\beta$, independent of γ, while the $\Delta\Omega(\omega^2) \approx \frac{\gamma(m_2-m_1)}{m_1m_2}$ when $\gamma \gg 2\beta$.

2. Period-two spring model

For the period-two spring model, β_n takes two values β_1, β_2 periodically, where $\beta_2 > \beta_1 > 0$. By analogy with Eq. (2), the equation of motion of the system with $2N$ atoms can be expressed as

$$\begin{aligned} m\ddot{\mu}_{2n} &= -\beta_1(\mu_{2n} - \mu_{2n-1}) + \beta_2(\mu_{2n+1} - \mu_{2n}) - \frac{\gamma}{N}\sum_{l=0}^{2N-1}(\mu_{2n} - \mu_l), \\ m\ddot{\mu}_{2n+1} &= -\beta_2(\mu_{2n+1} - \mu_{2n}) + \beta_1(\mu_{2n+2} - \mu_{2n+1}) - \frac{\gamma}{N}\sum_{l=0}^{2N-1}(\mu_{2n+1} - \mu_l). \end{aligned} \tag{A11}$$

The equations have the same lattice wave solution as Eq. (A2). Then, using a process similar to that for the period-two mass model, the frequency is obtained,

$$\omega_\pm^2(q) = \frac{D_3 \pm \sqrt{\left[D_4 + \gamma\delta_{q0}(\beta_1 + \beta_2)\cos q + \left(\frac{1}{2}\gamma\delta_{q0}\right)^2\right]}}{m}, \tag{A12}$$

where $D_3 = \beta_1 + \beta_2 + \frac{1}{2}\gamma$ and $D_4 = (\beta_1 + \beta_2)^2$ for $q = 0$, and $D_3 = \beta_1 + \beta_2 + \gamma$ and $D_4 = \beta_1^2 + \beta_2^2 + 2\beta_1\beta_2\cos 2q$ for $q \neq 0$.

For $q = 0$, the frequency is

$$\omega_\pm^2(q) = \frac{D_3 \pm D_3}{m} = \begin{cases} \dfrac{2\left(\beta_1 + \beta_2 + \frac{\gamma}{2}\right)}{m}, \\ 0. \end{cases} \tag{A13}$$

For $q \neq 0$, the frequency is

$$\omega^2 = \frac{(\beta_1 + \beta_2 + \gamma) \pm \sqrt{\beta_1^2 + \beta_2^2 + 2\beta_1\beta_2\cos 2q}}{m}. \tag{A14}$$

Similarly, the $\Delta G(\omega^2) = \omega_-^2(q \to 0) - \omega_-^2(q = 0)$ can be written as

$$\Delta G(\omega^2) = \frac{\gamma}{m}. \tag{A15}$$

And the $\Delta\Omega(\omega^2)$ is

$$\Delta\Omega(\omega^2) = \omega_+^2(q \to 0) - \omega_-^2(q \to 0) = \frac{2(\beta_1 + \beta_2)}{m}. \tag{A16}$$

It can be seen that the $\Delta\Omega(\omega^2)$ is independent of γ.

[1] P. W. Anderson, Phys. Rev. **109**, 1492 (1958).
[2] P. Dean, Proc. Phys. Soc. **84**, 727 (1964).
[3] N. Mott and W. Twose, Adv. Phys. **10**, 107 (1961).
[4] H. Matsuda and K. Ishii, Prog. Theor. Phys. Suppl. **45**, 56 (1970).
[5] K. Ishii, Prog. Theor. Phys. Suppl. **53**, 77 (1973).

[6] S. E. Burkov, B. E. C. Koltenbah, and L. W. Bruch, Phys. Rev. B **53**, 14179 (1996).
[7] M. Quilichini, Rev. Mod. Phys. **69**, 277 (1997).
[8] F. A. B. F. de Moura, L. P. Viana, and A. C. Frery, Phys. Rev. B **73**, 212302 (2006).
[9] J. C. Cressoni and M. L. Lyra, Phys. Rev. B **53**, 5067 (1996).
[10] P. K. Datta and K. Kundu, Phys. Rev. B **51**, 6287 (1995).
[11] A. Esmailpour, M. Esmailpour, A. Sheikhan, M. Elahi, M. R. R. Tabar, and M. Sahimi, Phys. Rev. B **78**, 134206 (2008).
[12] F. Domi'nguez-Adame, E. Macia, and A. Sanchez, Phys. Rev. B **48**, 6054 (1993).
[13] F. A. B. F. de Moura, M. D. Coutinho-Filho, E. P. Raposo, and M. L. Lyra, Phys. Rev. B **68**, 012202 (2003).
[14] F. Shahbazi, A. Bahraminasab, S. M. Vaez Allaei, M. Sahimi, and M. R. R. Tabar, Phys. Rev. Lett. **94**, 165505 (2005).
[15] A. E. B. Costa and F. A. B. F. de Moura, J. Phys.: Condens. Matter **23**, 065101 (2011).
[16] H. S. Yamada, Chaos Solitons Fractals **113**, 178 (2018).
[17] P. Tabeling, Phys. Rep. **362**, 1 (2002).
[18] H. J. H. Clercx and G. J. F. van Heijst, Appl. Mech. Rev. **62**, 020802 (2009).
[19] R. B. Griffiths, Phys. Rev. **176**, 655 (1968).
[20] S. S. Banerjee, R. B. Griffiths, and M. Widom, J. Stat. Phys. **93**, 109 (1998).
[21] P. Hertel and W. Thirring, Ann. Phys. **63**, 520 (1971).
[22] J. Barré, D. Mukamel, and S. Ruffo, Phys. Rev. Lett. **87**, 030601 (2001).
[23] P. H. Chavanis, Intl. J. Mod. Phys. B **20**, 3113 (2006).
[24] A. Campa, T. Dauxois, and S. Ruffo, Phys. Rep. **480**, 57 (2009).
[25] B. Žunkovič, M. Heyl, M. Knap, and A. Silva, Phys. Rev. Lett. **120**, 130601 (2018).
[26] M. Li, D. Zhirihin, M. Gorlach, X. Ni, D. Filonov, A. Slobozhanyuk, A. Alù, and A. B. Khanikaev, Nat. Photon. **14**, 89 (2020).
[27] M. Block, Y. Bao, S. Choi, E. Altman, and N. Y. Yao, Phys. Rev. Lett. **128**, 010604 (2022).
[28] P. A. Morais, J. S. Andrade, E. M. Nascimento, and M. L. Lyra, Phys. Rev. E **84**, 041110 (2011).
[29] J. Wang and A. C. Li, Phys. Rev. E **106**, 014135 (2022).
[30] S. Lepri, J. Stat. Phys. **190**, 16 (2023).
[31] H. Zhou, G. Zhang, J. S. Wang, and Y. W. Zhang, Phys. Rev. E **94**, 052123 (2016).
[32] P. Hauke and L. Tagliacozzo, Phys. Rev. Lett. **111**, 207202 (2013).
[33] F. Evers and A. D. Mirlin, Rev. Mod. Phys. **80**, 1355 (2008).
[34] L. F. Santos, F. Borgonovi, and G. L. Celardo, Phys. Rev. Lett. **116**, 250402 (2016).
[35] G. L. Celardo, R. Kaiser, and F. Borgonovi, Phys. Rev. B **94**, 144206 (2016).
[36] D. Sherrington and S. Kirkpatrick, Phys. Rev. Lett. **35**, 1792 (1975).
[37] H. Lipkin, N. Meshkov, and A. Glick, Nucl. Phys. **62**, 188 (1965).
[38] M. Antoni and S. Ruffo, Phys. Rev. E **52**, 2361 (1995).
[39] A. Friedenauer, H. Schmitz, J. T. Glueckert, D. Porras, and T. Schaetz, Nat. Phys. **4**, 757 (2008).
[40] J. W. Britton, B. C. Sawyer, A. C. Keith, C. C. J. Wang, J. K. Freericks, H. Uys, M. J. Biercuk, and J. J. Bollinger, Nature (London) **484**, 489 (2012).
[41] P. Jurcevic, B. P. Lanyon, P. Hauke, C. Hempel, P. Zoller, R. Blatt, and C. F. Roos, Nature (London) **511**, 202 (2014).
[42] J. S. Douglas, H. Habibian, C. L. Hung, A. V. Gorshkov, H. J. Kimble, and D. E. Chang, Nat. Photon. **9**, 326 (2015).
[43] W. Press, S. Teukolsky, W. Vetterling, and B. Flannery, *Numerical Recipes* (Cambridge University Press, Cambridge, 1992).
[44] For a finite N, the gap is well approximated by γ/m for $\gamma \gg \beta$.
[45] S. S. de Albuquerque, J. L. L. dos Santos, F. A. B. F. de Moura, and M. L. Lyra, J. Phys.: Condens. Matter **27**, 175401 (2015).